

Supporting Information

The effects of intercalated environmental gas molecules on the carrier dynamics in WSe₂/WS₂ heterostructures

Yanxue Zhang,^{‡a} Hongsheng Liu,^{‡a} Yanyan Zhao,^a Jiaqi Lin^{c*}, Yizhen Bai,^a Jijun Zhao^{*a,b},
Junfeng Gao^{*a,b}

^a Key laboratory of Materials Modification by Laser, Ion and Electron Beams (Dalian University of Technology), Ministry of Education, Dalian, 116024, China

^b State Key Laboratory of Structural Analysis for Industrial Equipment, Dalian University of Technology, Dalian, 116024, China

^c The School of Bioengineering, Dalian University of Technology, Dalian, 116024, China

[‡]These authors contributed equally to the work

Email: gaojf@dlut.edu.cn, zhaojj@dlut.edu.cn, jqlin@dlut.edu.cn

Table of contents

Computational methods	4
Figure S1. Band structures of optimized primitive cell of (a) WS ₂ and (b) WSe ₂ monolayer under 0%, 2% and 4% strain, respectively. The plus sign and minus sign denote tension and compression, respectively. The Fermi energy level is set as zero.	7
Figure S2. (a-b) Top and side views of optimized primitive cell of WSe ₂ /WS ₂ heterostructure. (c) Projected band structures of WSe ₂ /WS ₂ heterostructure. The color bar describes the contribution from WSe ₂ layer (red part) and WS ₂ layer (blue part), respectively.	8
Figure S3. (a-i) The initial and optimized structure of O ₂ molecule intercalated heterostructures.	9
Table S1. The bond lengths of O/W/S/Se-O bond and interlayer distance <i>d</i> for the optimized structure in Figure S3.....	10
Figure S4. The dissociation pathway and barrier of O ₂ molecule in the interlayer of WSe ₂ /WS ₂ heterostructure. The inset shows the top and side view of the structure of initial state (IS), transition state (TS) and final state (FS).	11
Figure S5. The charge density difference and the planar-average charge density difference along the Z direction of (a) pristine, (b) O ₂ intercalated, (c) H ₂ O intercalated and (d) N ₂ intercalated WSe ₂ /WS ₂ vdW heterostructures, respectively. The pink and green color represents the charge accumulation and depletion, respectively. The isosurface value is set as 0.0001 e /Bohr ³	12
Figure S6. (a-e) The optimized structure of H ₂ O intercalated WSe ₂ /WS ₂ vdW heterostructures.	13
Table S2. The bond lengths of O-H, S-H and Se-H and bond angle of HOH and <i>d</i> for the optimized structure in Figure S6.....	14
Figure S7. (a-d) The initial and optimized structure of N ₂ intercalated WSe ₂ /WS ₂ vdW heterostructures.	15

Table S3. The bond lengths of N-N, N-S, N-Se and d for the optimized structure in Figure S7. 16

Figure S8. (a) The top and side view of optimized bilayer WS₂. The primitive cell is marked by black dashed line. The initial (left panel) and optimized (right panel) structure of (b) O₂ intercalated, (c) H₂O intercalated and (d) N₂ intercalated bilayer WS₂, respectively.17

Figure S9. (a) The lattice of primitive cell (red line) and supercell (blue line) of WSe₂/WS₂ vdW heterostructure. (b) The corresponding high symmetric K points.18

Figure S10. The projected band structures of supercell and corresponding unfolding band structures for (a, b) pristine, (c, d) O₂ intercalated, (e, f) H₂O intercalated and (g, h) N₂ intercalated heterostructures. Blue, red and green color circles are states contributed by WS₂ layer, WSe₂ layer and intercalation molecule, respectively. The CBM band offset ΔE_c and VBM band offset ΔE_v is marked in (b).19

Table S4. The ΔE_c and ΔE_v of pristine, O₂ intercalated, H₂O intercalated and N₂ intercalated heterostructures.20

Figure S11. The time-dependent spatial electron localization on (a, i) pristine, (b, j) O₂ intercalated, (c, k) H₂O intercalated and (d, l) N₂ molecule intercalated WSe₂/WS₂ vdW heterostructures at 300 K and 78 K, respectively. The time-dependent electron energy of (e, m) pristine, (f, n) O₂ intercalated, (g, o) H₂O intercalated and (h, p) N₂ intercalated WSe₂/WS₂ vdW heterostructures at 300 K and 78 K, respectively. The color strips represent the distribution of electron on different energy level orbitals. The darker the color, the more electrons are distribution in this orbital. The blue dashed line denotes the average electron energy. The energy reference is the Fermi level of each system.21

Figure S12. The time-dependent spatial hole localization on (a, i) pristine, (b, j) O₂ intercalated, (c, k) H₂O intercalated and (d, l) N₂ molecule intercalated WSe₂/WS₂ vdW heterostructures at 300 K and 78 K, respectively. The time-dependent hole energy of (e, m) pristine, (f, n) O₂ intercalated, (g, o) H₂O intercalated and (h, p) N₂ intercalated WSe₂/WS₂ vdW heterostructures at 300 K and 78 K, respectively. The color strips represent the distribution of hole on different energy level orbitals. The darker the color, the more holes are distribution in this orbital. The blue dashed line denotes the average hole energy. The energy reference is the Fermi level of each system.23

Figure S13. The time-dependent electron population on (a, e) pristine, (b, f) O₂ intercalated, (c, g) H₂O intercalated and (d, h) N₂ molecule intercalated WSe₂/WS₂ vdW heterostructures at 300 K and 78 K, respectively.25

Figure S14. The time-dependent energy level evolution at Γ point of (a) pristine, (b) O₂ intercalated, (c) H₂O intercalated and (d) N₂ intercalated WSe₂/WS₂ vdW heterostructures at 78 K, respectively. The color bar in (a-d) represents the contribution from WSe₂ layer (red part) and WS₂ layer (blue part), respectively. Fourier transforms of the donor and relevant acceptor energy

states during the process of electron transfer and hole transfer in (e, i) pristine, (f, j) O₂ intercalated, (g, k) H₂O intercalated and (h, l) N₂ intercalated WSe₂/WS₂ vdW heterostructures at 78 K, respectively. The color bar in (e-l) represent the band number.26

Figure S15. The phonon spectra of (a) pristine, (b) O₂ intercalated, (c) H₂O intercalated and (d) N₂ intercalated heterostructures, respectively.....27

Figure S16. The averaged NAC values between the orbitals in the process of electron transfer, hole transfer and recombination in (a, e, i) pristine, (b, f, j) O₂ intercalated, (c, g, k) H₂O intercalated and (d, h, l) N₂ intercalated WSe₂/WS₂ vdW heterostructures at 78 K, respectively. Here, C+1, C+2, ... means CBM+1, CBM+2, ... level, respectively; V-1, V-2, ...means VBM-1, VBM-2, ... energy level, respectively.....28

Figure S17. The band gap distribution during MD simulation of pristine, O₂ intercalated, H₂O intercalated and N₂ intercalated WSe₂/WS₂ vdW heterostructures at (a) 300 K and (b) 78 K, respectively. The average PBE band gap values are labeled in the center.29

Figure S18. Fourier transforms of CBM and VBM of pristine, O₂ intercalated, H₂O intercalated and N₂ intercalated heterostructures at (a) 300 K and (b) 78 K, respectively.30

Figure S19. The RMSD of S, Se and W atoms during MD simulation of (a, e) pristine, (b, f) O₂ intercalated, (c, g) H₂O intercalated and (d, h) N₂ intercalated WSe₂/WS₂ vdW heterostructures at 300 K and 78 K, respectively.31

References.....32

Computational methods

Our first-principle calculations were performed using Vienna Ab Initio Simulation Package (VASP).¹ The projector augmented wave (PAW) scheme was used to describe the core electrons.² The exchange-related interaction was tackled by Perdew-Burke-Ernzerhof functional (PBE) within generalized gradient approximation (GGA).³ The DFT-D2 method was adopted to describe the weak van der Waals interactions.⁴ The plane wave energy cutoff was set as 500 eV. The convergence criteria of total energy and force were set at 10^{-5} eV and 0.001 eV/Å, respectively. A larger than 20 Å vacuum region was used to avoid the interaction of neighbor layer. The $12 \times 12 \times 1$ and $1 \times 1 \times 1$ Monkhorst k-point mesh was used for primitive cell and $3 \times 3 \times 1$ orthogonal supercell.⁵ All atoms were fully relaxed but the cell parameter is fixed.

The Γ point carrier dynamic process was based on the orthogonal $3 \times 3 \times 1$ supercell (pristine: 108 atoms, O₂ intercalation: 110 atoms, H₂O intercalation: 111 atoms, N₂ intercalation: 110 atoms), as showed in Figure 1a-de. The velocity rescaling method was used to heat pristine, O₂, H₂O and N₂ molecule intercalated WSe₂/WS₂ heterostructures to 300 K and 78 K, respectively. Then, *ab initio* nonadiabatic molecular dynamics (NAMD) simulations were carried out by using the Hefei-NAMD⁶ code. The fewest switches surface hopping (FSSH)⁷ method was used to investigated the process of electron and hole separation process. Since the quantum decoherence has a large influence on process with energy gap, the decoherence-induced surface hopping (DISH)⁸ method was used to study the recombination dynamic. For pristine heterostructure, 5 ps and 2 ns microcanonical *ab initio* molecular dynamics⁹ (AIMD) trajectories were generated with time step of 1 fs for electron hole separation and recombination simulation, respectively. Results of NAMD and DISH simulations were obtained by averaging over 100 and 50 different initial configurations, respectively. Then, for each selected structure, 20000 trajectories were sampled for last 3 ps for electron hole separation process, and 500 trajectories were sampled in 2 ns for the electron hole recombination simulation. For O₂ intercalated, H₂O intercalated and N₂ intercalated heterostructures, 5 ps and 2 ns microcanonical AIMD trajectories were generated with time step of 1 fs for carrier relaxation and recombination simulation, respectively. Results of NAMD and DISH simulation were obtained by averaging over 100 and 50 different initial structures, respectively. We sampled 20000 and 500 trajectories for last 2ps and 2 ns for the electron hole separation and recombination simulation, respectively.

To start the NAMD simulation electron transfer process, according to the CBM band offset, at 300 K, we set the following initial conditions. For pristine heterostructure, we set the photo-generated electron initially at CBM+21 (the CBM of WSe₂ layer) (CBM+13, 78K) as the electron donor state, and the CBM (the CBM of WS₂ layer) as the electron acceptor. For O₂ intercalated heterostructure, the photo-generated electron was initially set at CBM+30 (the CBM of WSe₂ layer) (CBM+27, 78K) as the electron donor state, and the CBM (the CBM of WS₂O₂ layer) as the electron acceptor. Since the intercalated O₂ spontaneously dissociates on the WS₂ surface, we argue that the O atoms to be an inseparable part of WS₂ and label it as WS₂O₂ in this paper. For H₂O intercalation heterostructure, we set the photo-generated electron initially localized at CBM+285 (the CBM of WSe₂ layer) (CBM+28, 78K) as the electron donor state and the CBM (the CBM of WS₂ layer) as the electron acceptor. For N₂ intercalation heterostructure, we set the photo-generated electron initially localized at CBM+18 (the CBM of WSe₂ layer) (CBM+19, 78K) as the electron donor state and the CBM (the CBM of WS₂ layer) as the electron acceptor.

Then, in hole transfer process, according to the VBM band offset, at 300K, we set the initial conditions as follows. For pristine heterostructure, we set the photo-generated hole initially at VBM-8 (the VBM of WS₂ layer) (VBM-10, 78K), which was the hole donor state, and the VBM (the VBM of WSe₂ layer) was set as the hole acceptor. For O₂ intercalated heterostructure, the photo-generated hole was initially set at VBM-13 (the VBM of WS₂O₂ layer) (VBM-13, 78 K), which was the hole donor state, and the VBM (the VBM of WSe₂ layer) as the hole acceptor. For H₂O intercalation heterostructure, the photo-generated hole was initially localized at VBM-15 (the VBM of WS₂ layer) (VBM-13, 78K), which was set as the hole donor state, and the VBM (the VBM of WSe₂ layer) was set as the hole acceptor. For N₂ intercalation heterostructure, the photo-generated hole was initially localized at VBM-10 (the VBM of WS₂ layer) (VBM-10, 78 K), which was set as the hole donor state, and the VBM (the VBM of WSe₂ layer) was set as the hole acceptor.

In the recombination process of pristine, O₂ and H₂O and N₂ intercalated heterostructures, we initiate the photo-generated electron localized in the CBM of the whole system, which is the electron donor state, and set the VBM of the whole system as the hole acceptor.

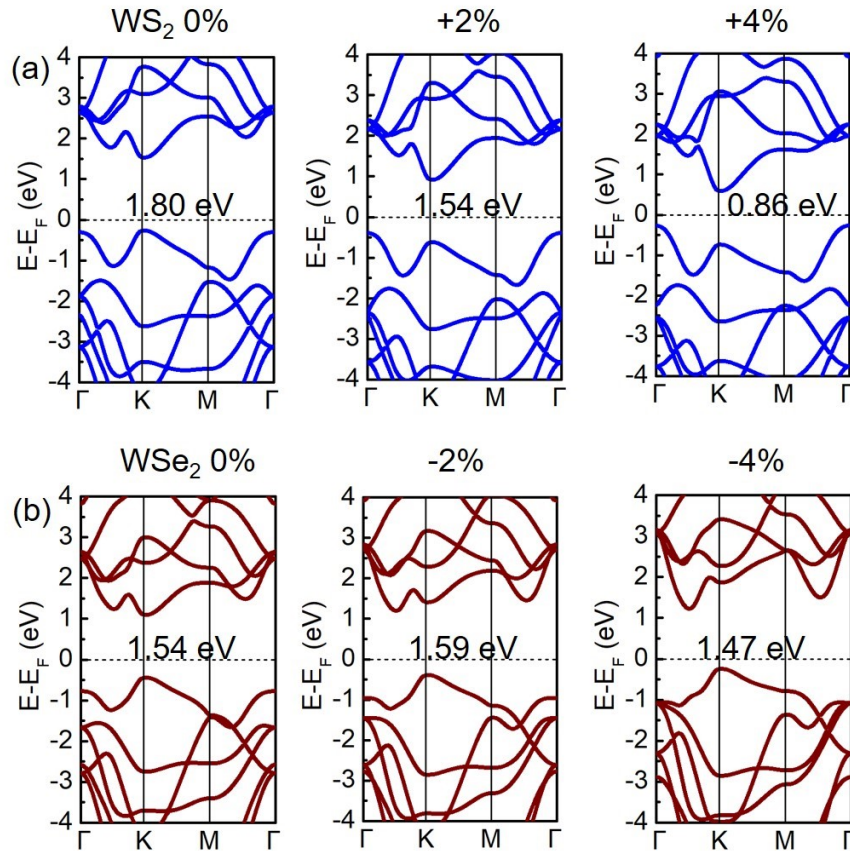


Figure S1. Band structures of optimized primitive cell of (a) WS₂ and (b) WSe₂ monolayer under 0%, 2% and 4% strain, respectively. The plus sign and minus sign denote tension and compression, respectively. The Fermi energy level is set as zero.

In order to reduce the lattice mismatch, the lattice constant of WSe₂/WS₂ heterostructure is set to be the average value of the lattice constants of WSe₂ and WS₂. WSe₂ layer is compressed by 2% and the WS₂ layer is stretched by 2%. To check the strain effect on the band gap, we calculated the band structures of WSe₂ and WS₂ monolayers with different strain as shown in Figure S1. The results show that strain of 4% has great effect on the band gap. Fortunately, strain of 2% has only small effect on the band gap. Therefore, deformation of both layers is a good choice to maintain the band gap.

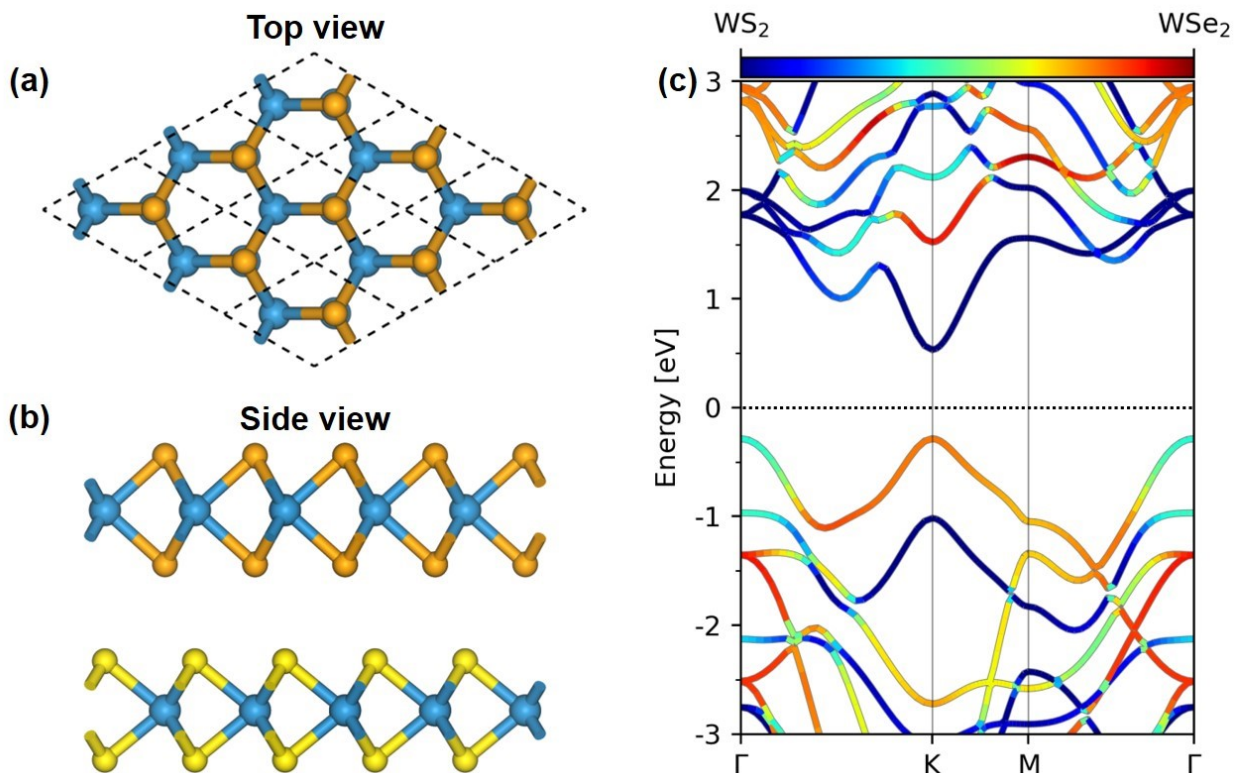


Figure S2. (a-b) Top and side views of optimized primitive cell of WSe_2/WS_2 heterostructure. (c) Projected band structures of WSe_2/WS_2 heterostructure. The color bar describes the contribution from WSe_2 layer (red part) and WS_2 layer (blue part), respectively.

According to the orbital projected band structures in Figure S2 for pristine WSe_2/WS_2 vdW heterostructure, the valence band maximum (VBM) mainly originates from WSe_2 and the conduction band minimum (CBM) mainly comes from WS_2 . Therefore, WSe_2/WS_2 vdW heterostructures exhibit typical type-II band alignment, which is promising for photocatalysts and solar cell due to the easy separation of photo-generated electron-hole pairs.

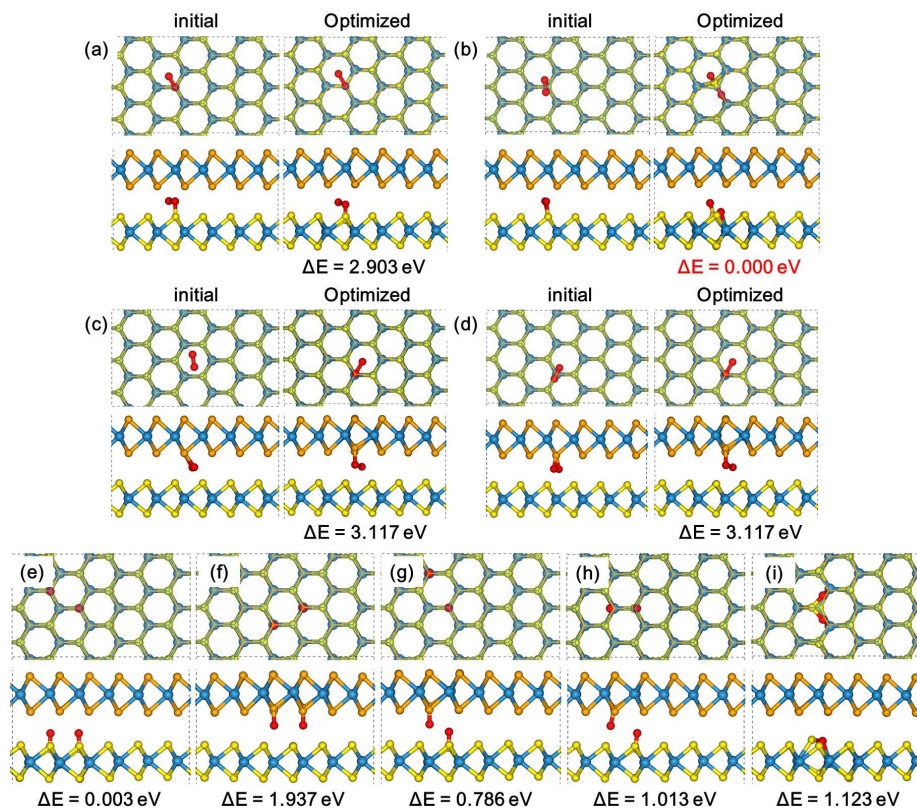


Figure S3. (a-i) The initial and optimized structure of O_2 molecule intercalated heterostructures.

We tested three cases, molecule initial located at the interlayer site, initial adsorption on WS_2 layer and initial adsorption on WSe_2 layer. Intercalation at different positions in the interlayer of WSe_2/WS_2 heterostructure for O_2 has shown in the Figure S3. As shown in Figure S3, O_2 molecule are more likely adsorbed and dissociated on WS_2 layer.

Table S1. The bond lengths of O/W/S/Se-O bond and interlayer distance d for the optimized structure in Figure S3.

System	Pristine	Vacuum	a	b	c	d
O-O (Å)	-	1.233	1.485	2.417	1.440	1.440
d (Å)	3.054	-	3.123	3.124	3.102	3.104
System	e	f	g	h	i	b
W-O (Å)	-	-	-	-	2.073	2.114
S-O (Å)	1.474	-	1.479	1.476	1.544	1.463/1.535
Se-O (Å)	-	1.662	1.670	1.672	-	-
d (Å)	3.104	3.126	3.11	3.111	3.152	3.124

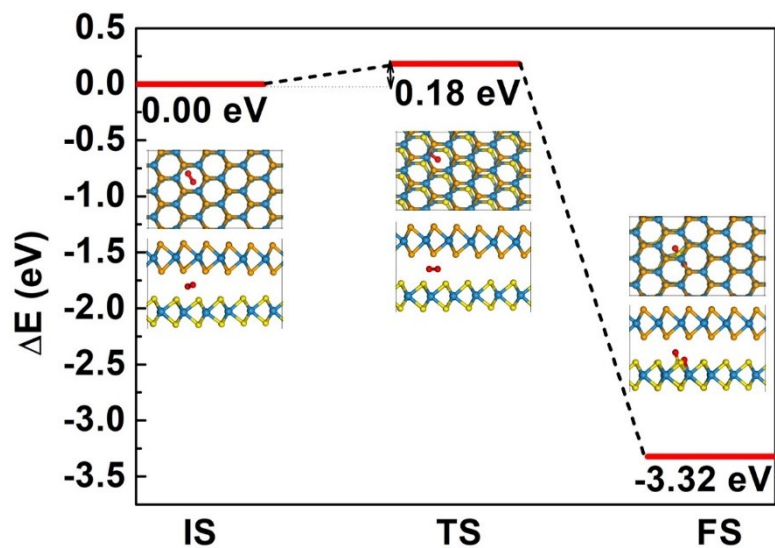


Figure S4. The dissociation pathway and barrier of O₂ molecule in the interlayer of WSe₂/WS₂ heterostructure. The inset shows the top and side view of the structure of initial state (IS), transition state (TS) and final state (FS).

The energy barrier for the O₂ dissociation in interlayer of WSe₂/WS₂ heterostructure is 0.18 eV, according to the CI-NEB calculation as shown in Figure S4.

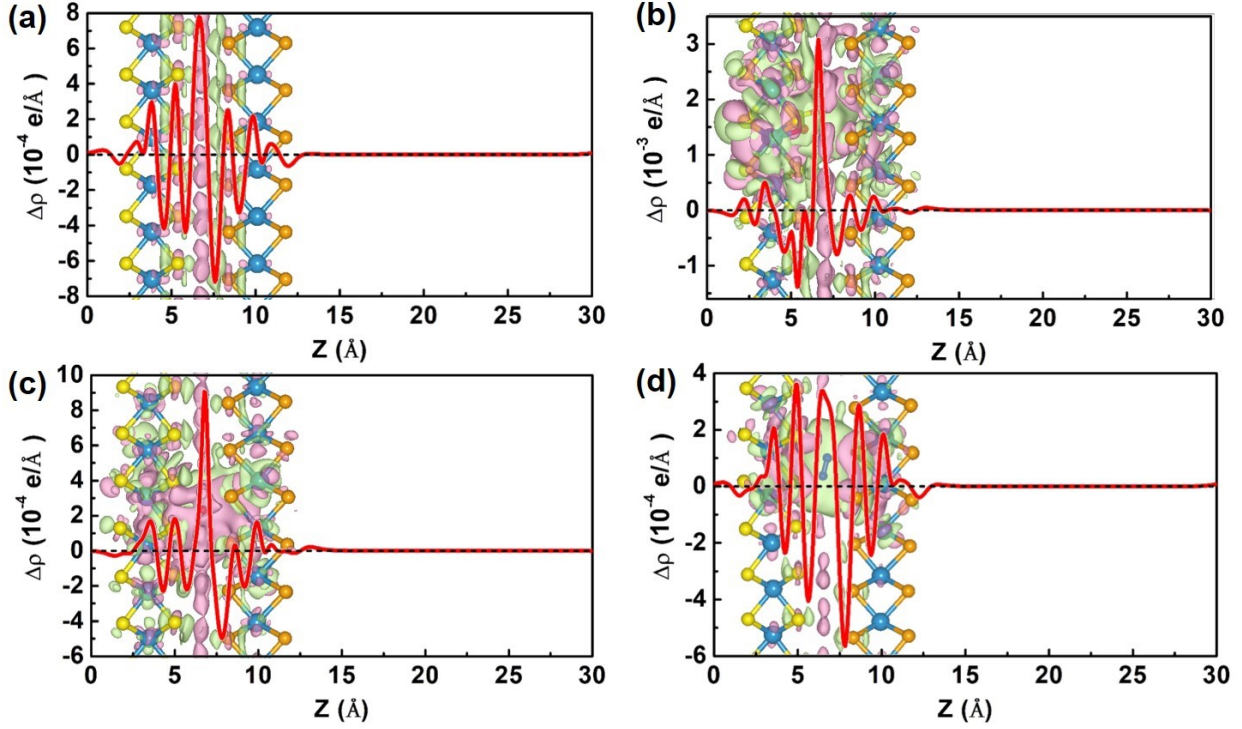


Figure S5. The charge density difference and the planar-average charge density difference along the Z direction of (a) pristine, (b) O₂ intercalated, (c) H₂O intercalated and (d) N₂ intercalated WSe₂/WS₂ vdW heterostructures, respectively. The pink and green color represents the charge accumulation and depletion, respectively. The isosurface value is set as 0.0001 |e|/Bohr³.

The confinement environment does activate O₂, H₂O and N₂ molecules, which can be understood by analyzing the charge transfer. The charge density difference ($\Delta\rho$) was calculated as follows,

$$\Delta\rho = \rho_{\text{total}} - \rho_{\text{WSe}_2} - \rho_{\text{WS}_2} - \rho_{\text{O}_2/\text{H}_2\text{O}/\text{N}_2} \quad (1)$$

where ρ_{total} , ρ_{WSe_2} , ρ_{WS_2} and $\rho_{\text{O}_2/\text{H}_2\text{O}/\text{N}_2}$ denote the charge density of heterostructure, monolayer WSe₂, monolayer WS₂, two O atoms and H₂O and N₂ molecule, respectively.

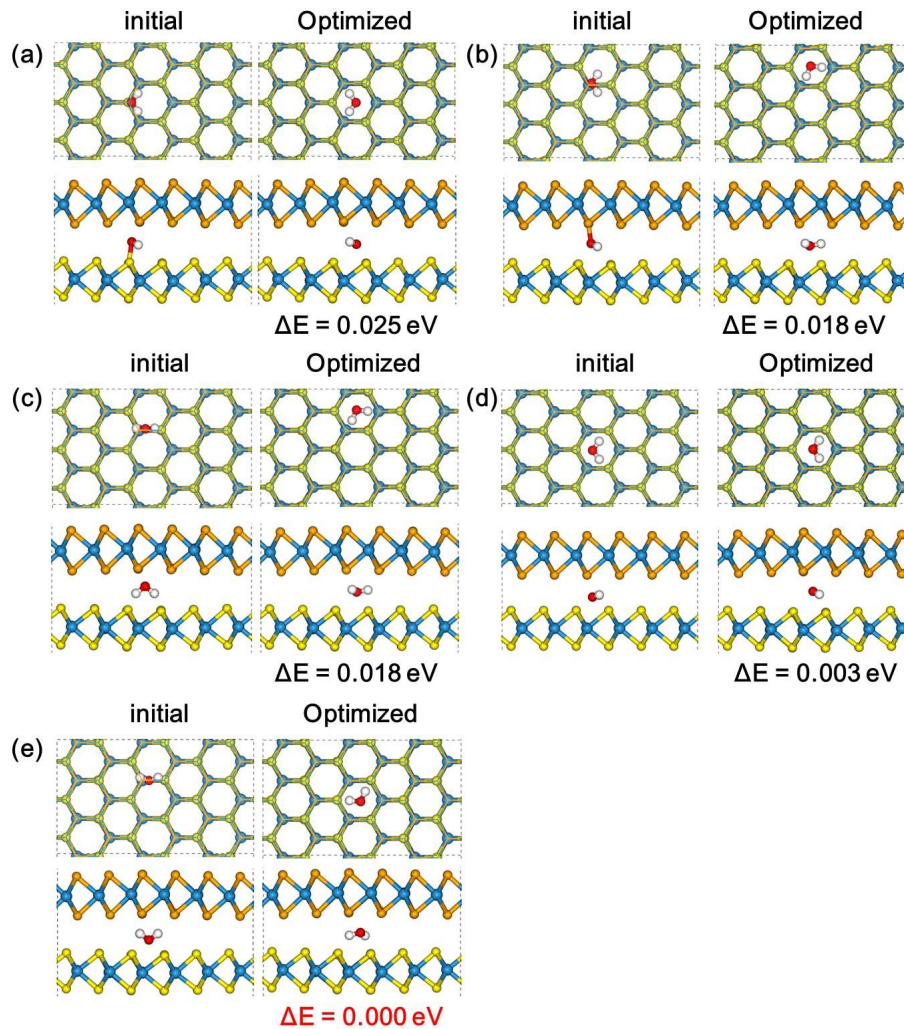


Figure S6. (a-e) The optimized structure of H₂O intercalated WSe₂/WS₂ vdW heterostructures.

We tested three cases, molecule initial located at the interlayer site, initial adsorption on WS₂ layer and initial adsorption on WSe₂ layer. Intercalation at different positions in the interlayer of WSe₂/WS₂ heterostructure for H₂O has shown in the Figure S6. As shown in Figure S6, the H₂O molecule prefers to locate at the hollow site independent of initial configurations. The two H atoms of H₂O molecule tend to be closer to S atoms of the WS₂ layer.

Table S2. The bond lengths of O-H, S-H and Se-H and bond angle of HOH and *d* for the optimized structure in Figure S6.

System	Vacuum	a	b	c	d	e
O-H (Å)	0.972	0.983	0.982/0.983	0.985	0.984/0.985	0.983
S-H (Å)	-	-	-	-	1.950/1.954	1.950/1.954
Se-H (Å)	-	2.084	2.083	2.082/2.083	-	-
∠HOH (°)	104.553	104.085	104.008	104.203	104.171	104.012
<i>d</i> (Å)	-	3.189	3.184	3.184	3.182	3.180

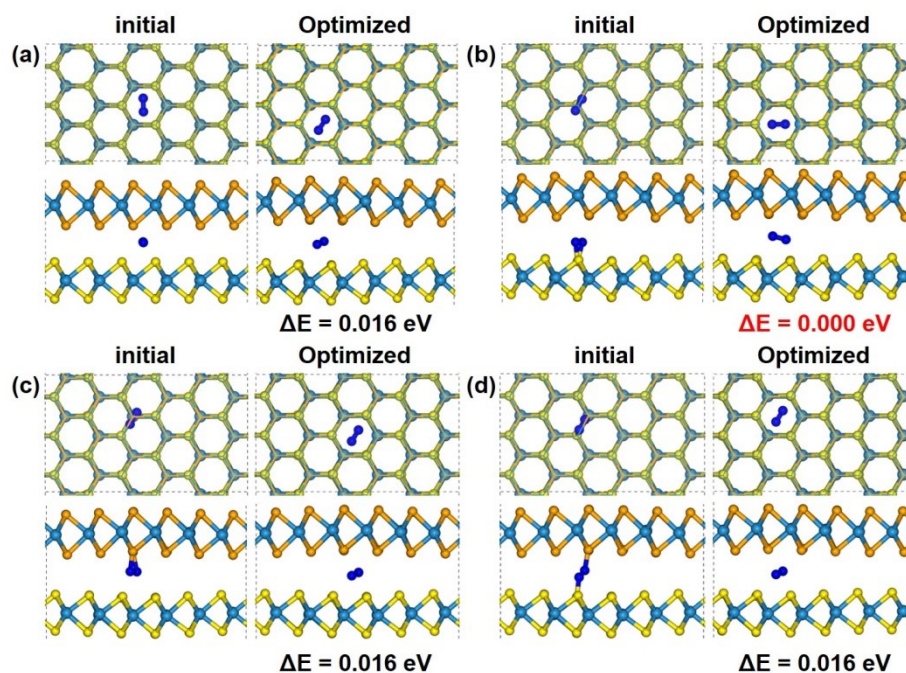


Figure S7. (a-d) The initial and optimized structure of N_2 intercalated WSe_2/WS_2 vdW heterostructures.

We tested three cases, molecule initial located at the interlayer site, initial adsorption on WS_2 layer and initial adsorption on WSe_2 layer. Intercalation at different positions in the interlayer of WSe_2/WS_2 heterostructure for N_2 has shown in the Figure S7. As shown in Figure S7, the N_2 molecule prefers to locate at the hollow site after optimization independent of initial configurations.

Table S3. The bond lengths of N-N, N-S, N-Se and *d* for the optimized structure in Figure S7.

System	Vacuum	a	b	c	d
N-N (Å)	1.114	1.125	1.125	1.125	1.125
N-S (Å)	-	2.493 (2.534)	2.518 (2.515)	2.482 (2.524)	2.487 (2.526)
N-Se (Å)	-	2.561 (2.604)	2.570 (2.594)	2.565 (2.595)	2.557 (2.597)
<i>d</i> (Å)	-	3.373	3.371	3.351	3.359

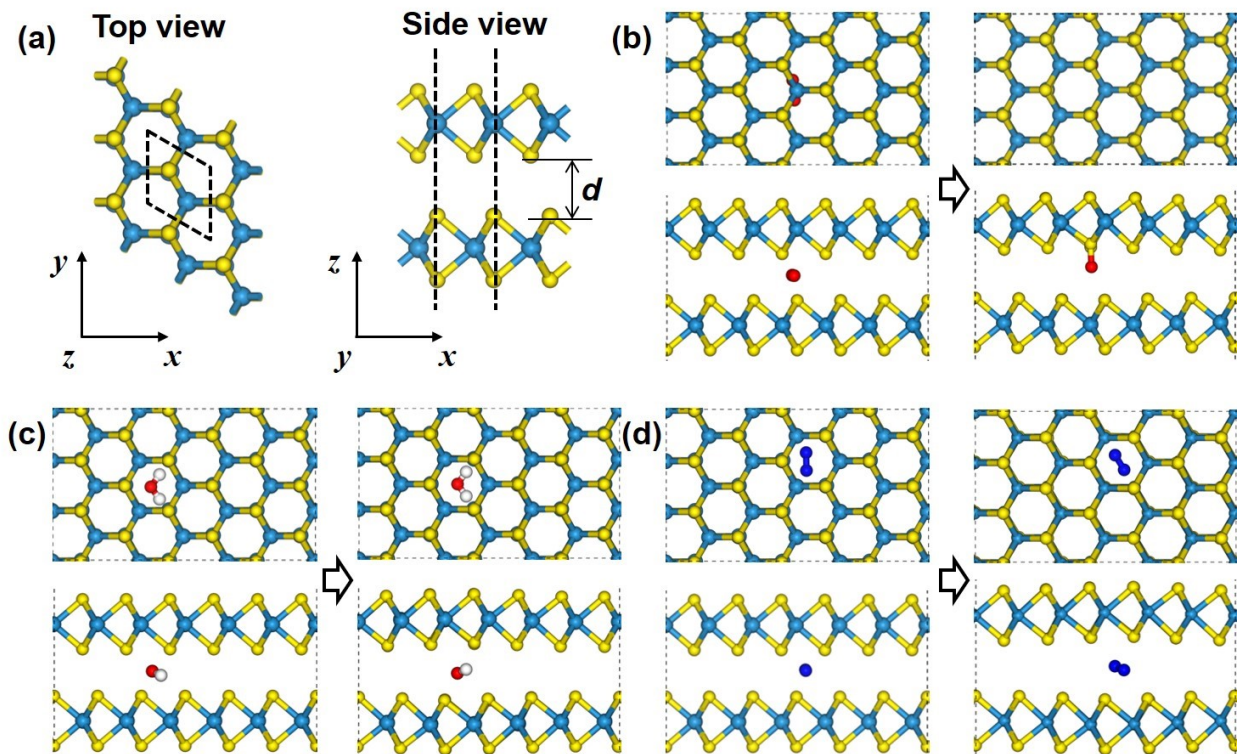


Figure S8. (a) The top and side view of optimized bilayer WS_2 . The primitive cell is marked by black dashed line. The initial (left panel) and optimized (right panel) structure of (b) O_2 intercalated, (c) H_2O intercalated and (d) N_2 intercalated bilayer WS_2 , respectively.

Whether it is strain that causes O_2 dissociation is unclear. To examine this, the O_2 , H_2O and N_2 intercalation in unstrained bilayer WS_2 layer with 2H stacking was investigated as shown in Figure S8. Similar to the case of the intercalation in WSe_2/WS_2 heterostructure, in the bilayer WS_2 , O_2 tends to dissociate while H_2O and N_2 keeps intact. Therefore, the strain effect on the dissociation of O_2 molecule can be excluded.

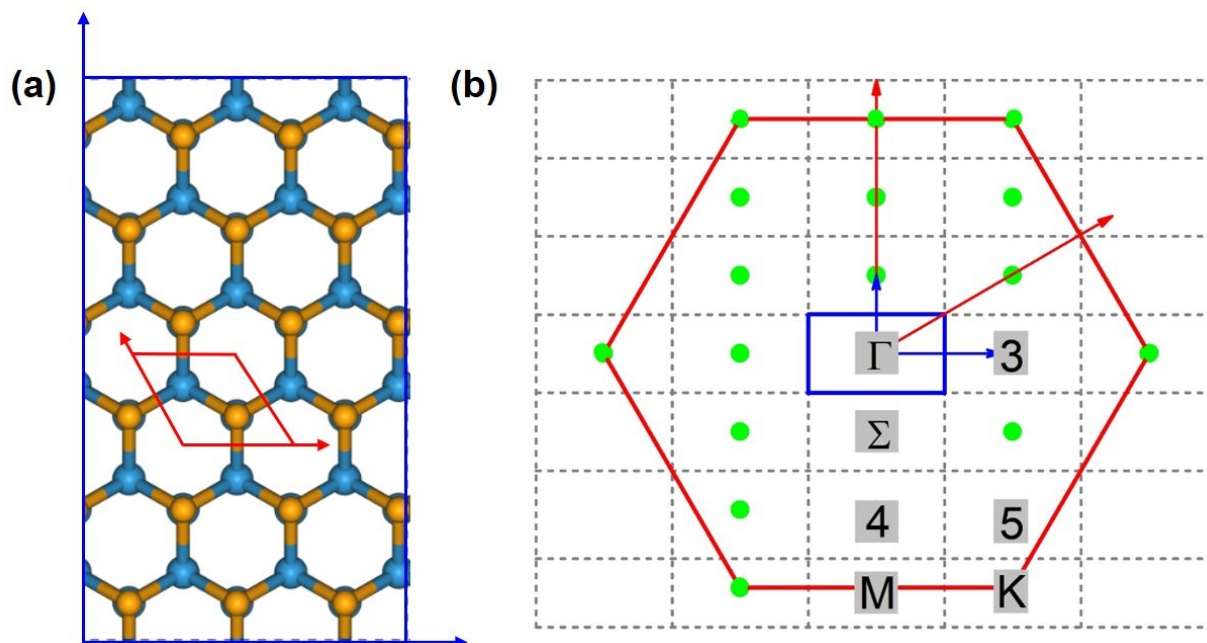


Figure S9. (a) The lattice of primitive cell (red line) and supercell (blue line) of WSe_2/WS_2 vdW heterostructure. (b) The corresponding high symmetric K points.

The large supercell induced band folding containing seven irreducible K points as show in Figure S9.

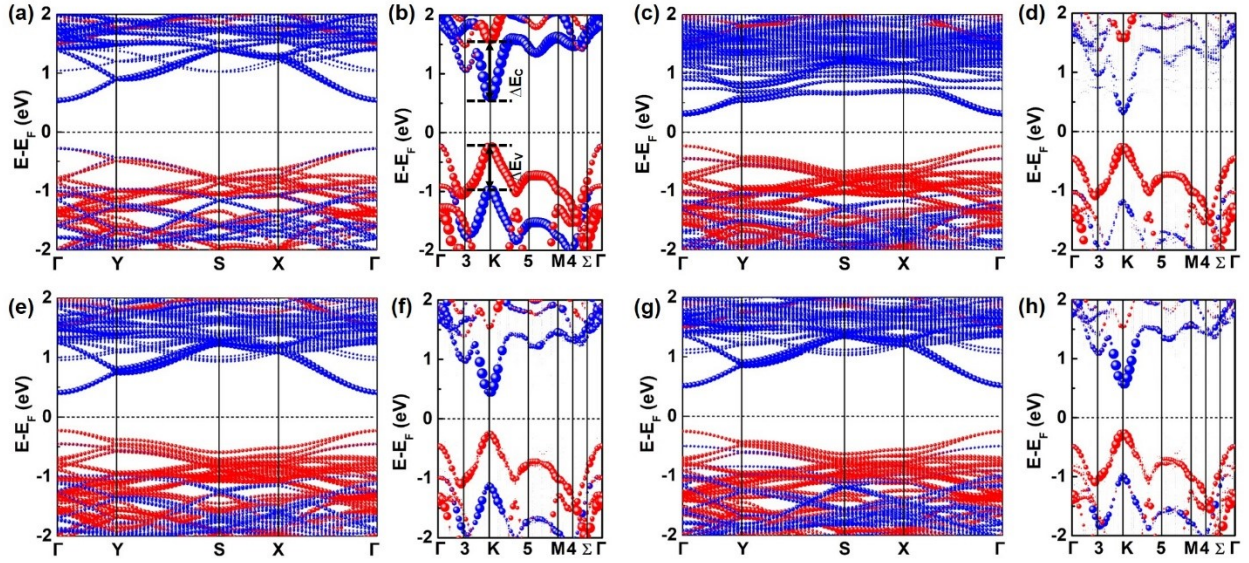


Figure S10. The projected band structures of supercell and corresponding unfolding band structures for (a, b) pristine, (c, d) O_2 intercalated, (e, f) H_2O intercalated and (g, h) N_2 intercalated heterostructures. Blue, red and green color circles are states contributed by WS_2 layer, WSe_2 layer and intercalation molecule, respectively. The CBM band offset ΔE_C and VBM band offset ΔE_V is marked in (b).

In order to clearly show the changes of band edge position, the band structures of pristine, O_2 intercalated, H_2O intercalated and N_2 intercalated WSe_2/WS_2 heterostructures are unfolded as shown in Figure S10b, d, f, h, respectively. Compared with the pristine heterostructure, the CBM band offset ΔE_C between the CBM at K of WS_2 (CB- $WS_2@K$) state and the CBM at K of WSe_2 (CB- $WSe_2@K$) state increased after molecule intercalation. The VBM at Γ of WSe_2 (VB- $WSe_2@I$) state moved down after molecule intercalation. The VBM at K of WS_2 (VB- $WS_2@K$) state also shifted down. Correspondingly, the VBM band offset ΔE_V between VB- $WS_2@K$ state and VB- $WSe_2@K$ state increased after molecule intercalation. The ΔE_C and ΔE_V of pristine, O_2 intercalated, H_2O intercalated and N_2 intercalated heterostructures are summarized in Table S4.

Table S4. The ΔE_c and ΔE_v of pristine, O₂ intercalated, H₂O intercalated and N₂ intercalated heterostructures.

System	WSe₂/WS₂	 O₂ 	 H₂O 	 N₂
ΔE_c (eV)	0.73	0.94	0.88	0.74
ΔE_v (eV)	0.98	1.25	1.14	1.00

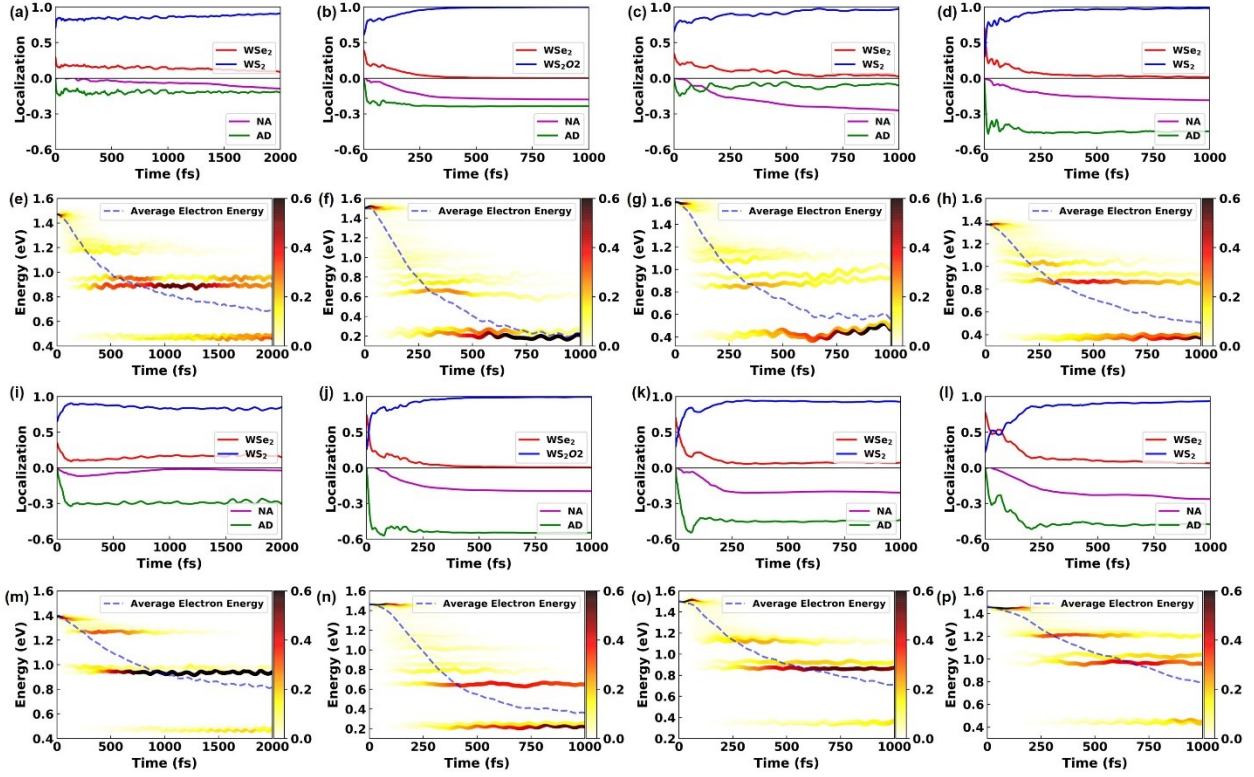


Figure S11. The time-dependent spatial electron localization on (a, i) pristine, (b, j) O_2 intercalated, (c, k) H_2O intercalated and (d, l) N_2 molecule intercalated WSe_2/WS_2 vdW heterostructures at 300 K and 78 K, respectively. The time-dependent electron energy of (e, m) pristine, (f, n) O_2 intercalated, (g, o) H_2O intercalated and (h, p) N_2 intercalated WSe_2/WS_2 vdW heterostructures at 300 K and 78 K, respectively. The color strips represent the distribution of electron on different energy level orbitals. The darker the color, the more electrons are distribution in this orbital. The blue dashed line denotes the average electron energy. The energy reference is the Fermi level of each system.

Figure S11i-p is the time dependent electron localization on two layers and electron energy change of pristine, O_2 intercalated, H_2O intercalated and N_2 intercalated heterostructures at 78 K, respectively. For pristine, O_2 intercalated, H_2O intercalated and N_2 intercalated heterostructures, the initial electron population on WSe_2 layer is 35%, 74%, 70%, 77%, respectively. Then a fast charge transfer from WSe_2 to WS_2 layer occurs and the electron population on WSe_2 layer reduces to 9%, 23%, 15%, 47% within 124 fs, 27 fs, 68 fs, 29 fs, respectively. AD mechanism contributes the fast charge transfer process. Note that the fast stage is still slower than the 300 K indicating that the AD mechanism depends on temperature. Subsequently, the electron population on WSe_2 layer slowly decreased and converged to 15%, 0%, 7% and 6%, respectively. This process is contributed by both AD and NA mechanism. The average electron energy of pristine, H_2O intercalated and N_2 intercalated heterostructure is not converged to CB- $WS_2@K$ state within 1ps, while the average electron energy of O_2 intercalated heterostructure is close to

the CB-WS₂@K state indicating O₂ intercalated promote the intervalley electron transfer from CB-WSe₂@K state to CB-WS₂@K state.

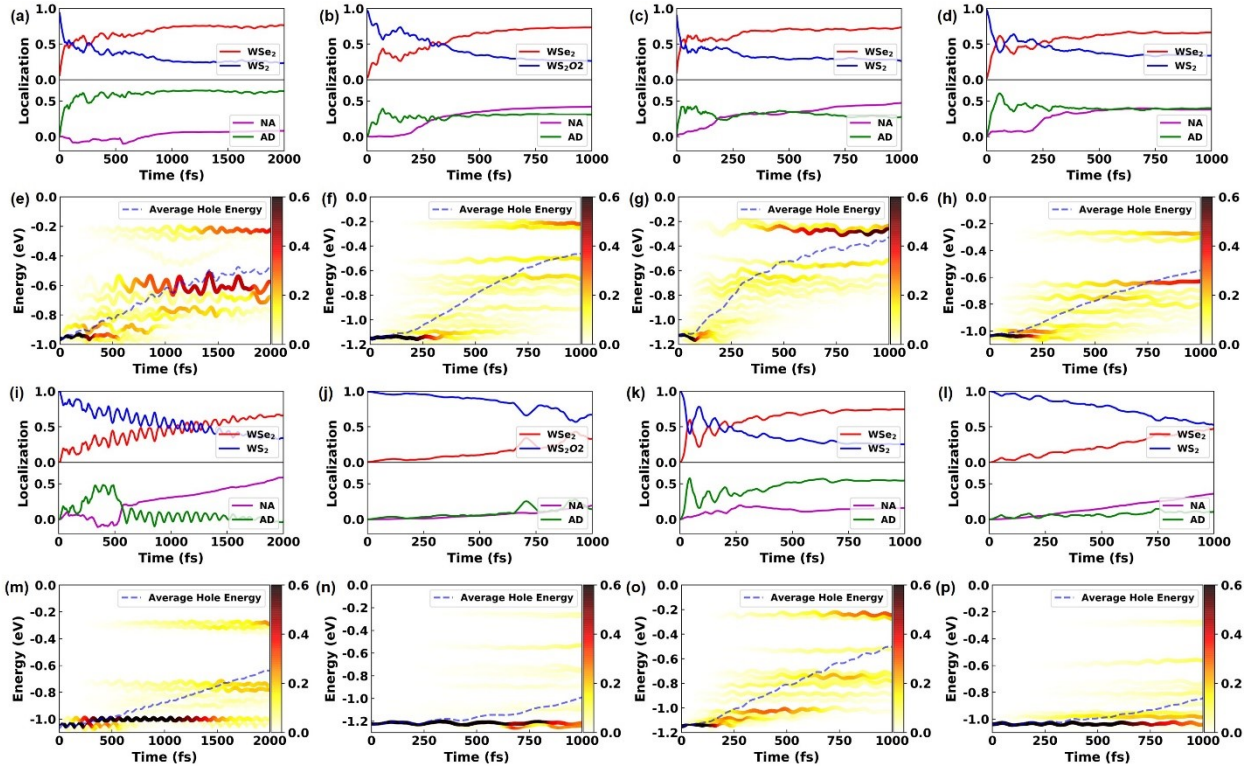


Figure S12. The time-dependent spatial hole localization on (a, i) pristine, (b, j) O_2 intercalated, (c, k) H_2O intercalated and (d, l) N_2 molecule intercalated WSe_2/WS_2 vdW heterostructures at 300 K and 78 K, respectively. The time-dependent hole energy of (e, m) pristine, (f, n) O_2 intercalated, (g, o) H_2O intercalated and (h, p) N_2 intercalated WSe_2/WS_2 vdW heterostructures at 300 K and 78 K, respectively. The color strips represent the distribution of hole on different energy level orbitals. The darker the color, the more holes are distribution in this orbital. The blue dashed line denotes the average hole energy. The energy reference is the Fermi level of each system.

Figure S12i-p is the time dependent hole population and hole energy change of pristine, O_2 , H_2O and N_2 intercalated WSe_2/WS_2 heterostructures at 78 K, respectively. The hole transfer process for pristine, O_2 intercalated and N_2 intercalated heterostructures are significantly slower than that at 300 K as shown in Figure S12i,j,l and Figure S12a,b,d. The initial hole population on WS_2 layer of pristine, O_2 intercalated and N_2 intercalated heterostructure is 100%. After 1ps, the hole population on WS_2 layer slowly reduced to 54%, 67% and 53%, respectively. NA mechanism dominates the slow process indicating that the NA mechanism depends on temperature. For the case of H_2O intercalated, the initial hole population on WS_2 layer is 100%. A fast hole transfer occurs within 33 fs, where the hole population on WS_2 layer is reduced to 50%. In this process, AD dominates the fast hole transfer process. After 1ps, the hole population on WS_2 layer slowly decreased and converged to 25%. As shown in Figure S12m,n,p, the average hole energy is nearly unchanged within 1 ps for pristine, O_2 intercalated and N_2 intercalated heterostructures. While the average hole energy of H_2O intercalated heterostructure

reached the VB-WSe₂@ Γ state within 1ps, indicating H₂O intercalation promotes the hole transfer from VB-WS₂@K state to VB-WSe₂@ Γ state.

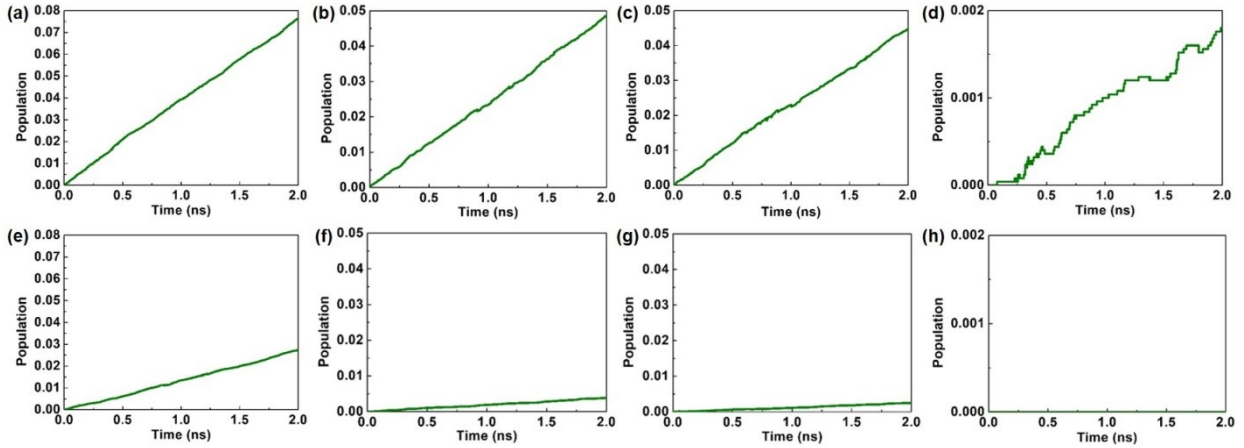


Figure S13. The time-dependent electron population on (a, e) pristine, (b, f) O_2 intercalated, (c, g) H_2O intercalated and (d, h) N_2 molecule intercalated WSe_2/WS_2 vdW heterostructures at 300 K and 78 K, respectively.

Figure S13e-h is the time dependent electron population on the VBM of pristine, O_2 intercalated, H_2O intercalated and N_2 intercalated heterostructures at 78 K, respectively. At 78 K, only 2.7%, 0.4%, 0.2%, and 0% electrons are relaxed from CBM to VBM within 2 ns for pristine, O_2 , H_2O and N_2 intercalated heterostructures, respectively. Note that the recombination rate in molecule intercalated heterostructure is still slower than that in pristine heterostructure. In particular, the recombination in N_2 intercalated heterostructure is totally suppressed at 78 K.

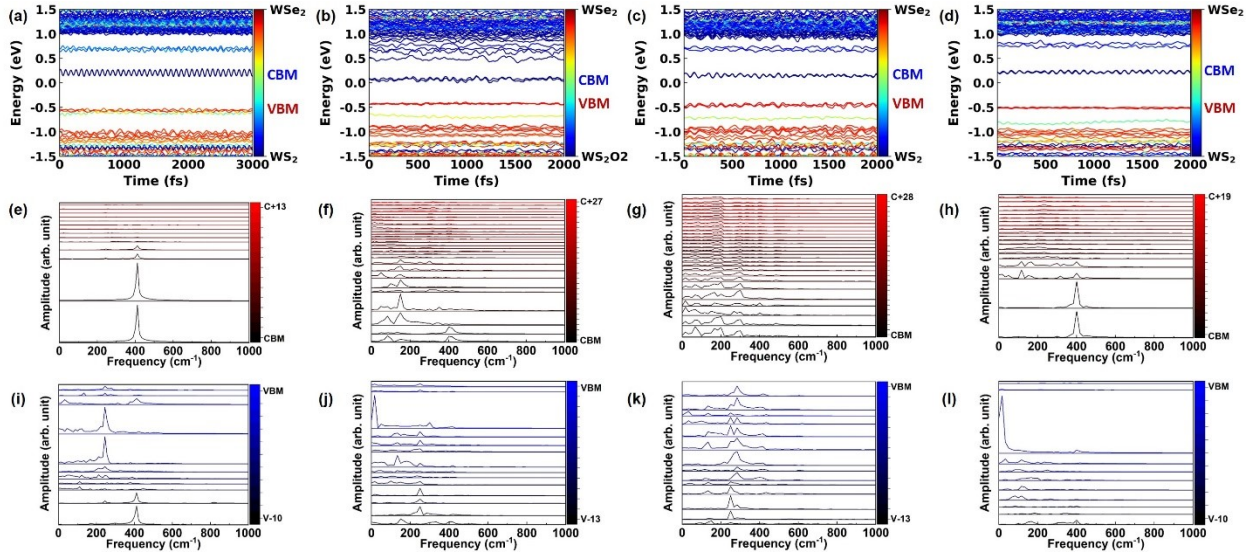


Figure S14. The time-dependent energy level evolution at Γ point of (a) pristine, (b) O_2 intercalated, (c) H_2O intercalated and (d) N_2 intercalated WSe_2/WS_2 vdW heterostructures at 78 K, respectively. The color bar in (a-d) represents the contribution from WSe_2 layer (red part) and WS_2 layer (blue part), respectively. Fourier transforms of the donor and relevant acceptor energy states during the process of electron transfer and hole transfer in (e, i) pristine, (f, j) O_2 intercalated, (g, k) H_2O intercalated and (h, l) N_2 intercalated WSe_2/WS_2 vdW heterostructures at 78 K, respectively. The color bar in (e-l) represent the band number.

The time dependent energy level evolution of pristine, O_2 intercalated, H_2O intercalated and N_2 intercalated heterostructures at 78 K is shown in Figure S14a-d. It can be seen that the energy state oscillation amplitude at 78 K is weaker than that at 300 K. The smaller fluctuation of energy states is because thermal excited nuclear motion at 78 K is weaker than that at 300 K. Except for O_2 intercalation, CBM+3 level and CBM+4 level is gapped, which slows the electron transfer process. In the hole transfer process, the donor state is gapped with acceptor for pristine, O_2 intercalated and N_2 intercalated heterostructures which suppressed hole transfer. For H_2O intercalated heterostructure, the donor state and acceptor state have significant orbital hybridization, which promotes the fast hole transfer.

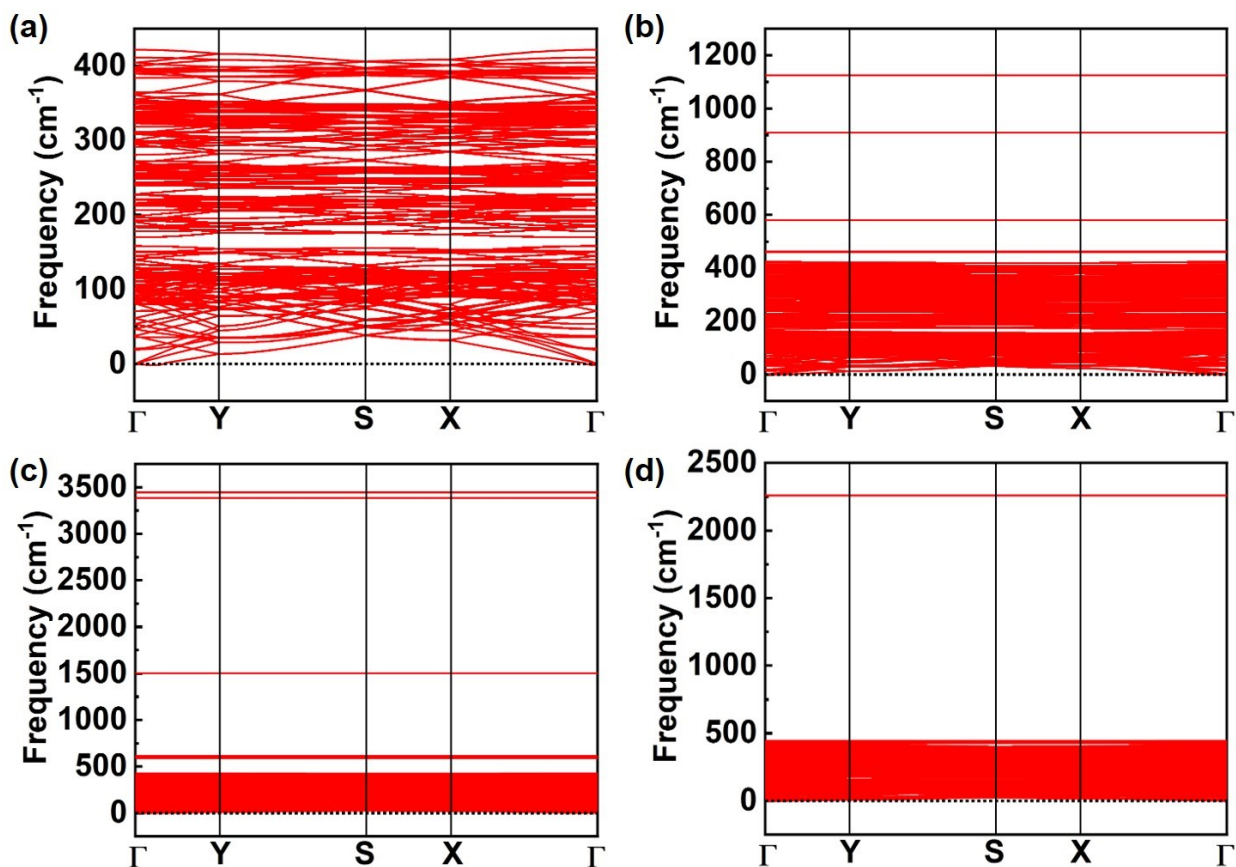


Figure S15. The phonon spectra of (a) pristine, (b) O₂ intercalated, (c) H₂O intercalated and (d) N₂ intercalated heterostructures, respectively.

The phonon spectra of pristine, O₂ intercalated, H₂O intercalated and N₂ intercalated WSe₂/WS₂ heterostructures were computed using the finite displacement approach with a $1 \times 1 \times 1$ supercell and a $1 \times 1 \times 1$ k-point grid, as implemented in the PHONOPY code.¹⁰ As shown in Figure S15a-d, molecule intercalation induces high frequency phonons.

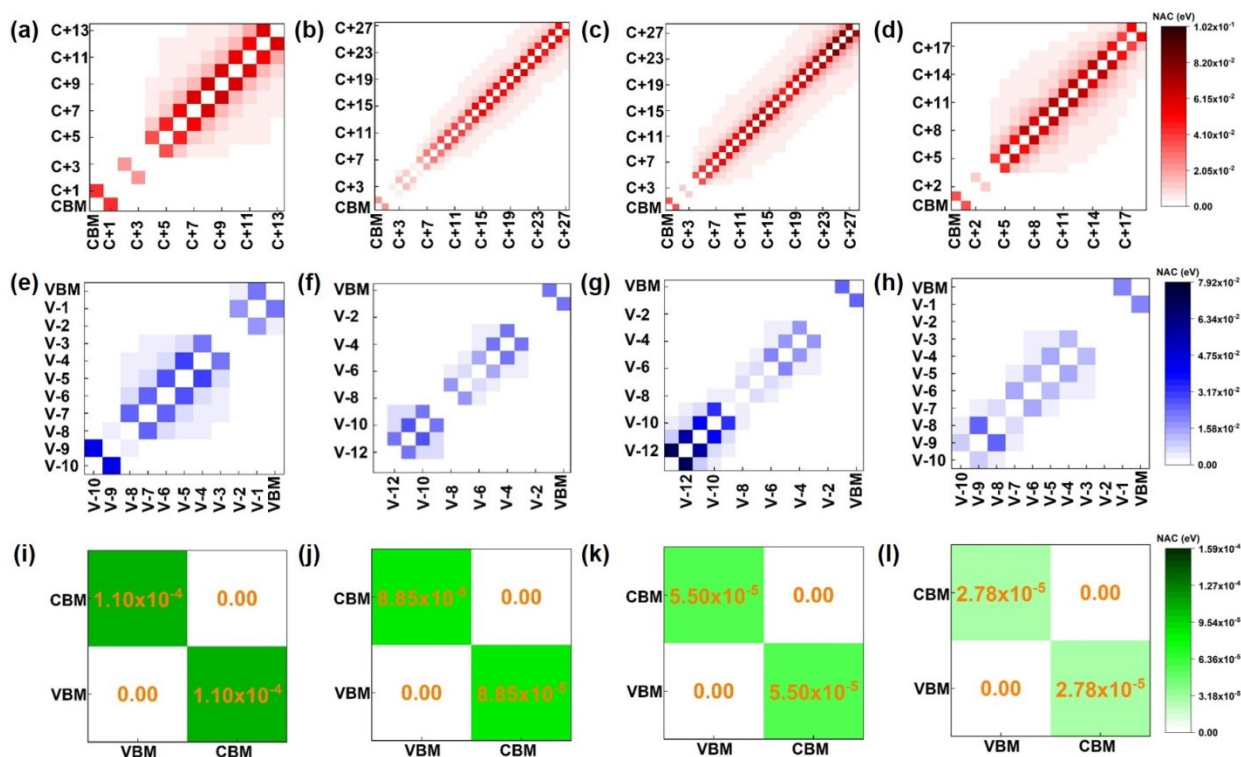


Figure S16. The averaged NAC values between the orbitals in the process of electron transfer, hole transfer and recombination in (a, e, i) pristine, (b, f, j) O₂ intercalated, (c, g, k) H₂O intercalated and (d, h, l) N₂ intercalated WSe₂/WS₂ vdW heterostructures at 78 K, respectively. Here, C+1, C+2, ... means CBM+1, CBM+2, ... level, respectively; V-1, V-2, ... means VBM-1, VBM-2, ... energy level, respectively.

At lower temperature of 78 K, the average NAC values become smaller than that at 300 K as shown in Figure S16. Thus, at low temperature the process of electron and hole transfer as well as recombination slows down. It is note that, at 78 K, the average NAC values between CBM and VBM of molecule intercalated heterostructures are still smaller than that in pristine heterostructures, which is consistent with the results of Figure S13e-h. The average band gaps of pristine, O₂ intercalated, H₂O intercalated and N₂ intercalated heterostructures at 78 K are 0.76 eV, 0.48 eV, 0.59 eV and 0.72 eV as shown in Figure S17b, indicating that the energy difference is not the main factor. The relative phonon amplitude of CBM and VBM state of pristine, O₂ intercalated, H₂O intercalated and N₂ intercalated heterostructures at 78 K is shown in Figure S18b. After molecule intercalation, the phonon amplitude of CBM state and VBM state is reduced significantly compared with pristine heterostructure, indicating the smaller phonon occupation and weaker electron-phonon coupling element. The RMSD of pristine, O₂, H₂O and N₂ intercalated heterostructures at 78 K are shown in Figure S19e-h. Molecule intercalation increases RMSD, indicating larger nuclear velocity. Thus, the reduced electron-phonon coupling element of CBM state and VBM state in molecule intercalation heterostructure is the main factor for the smaller average NAC value.

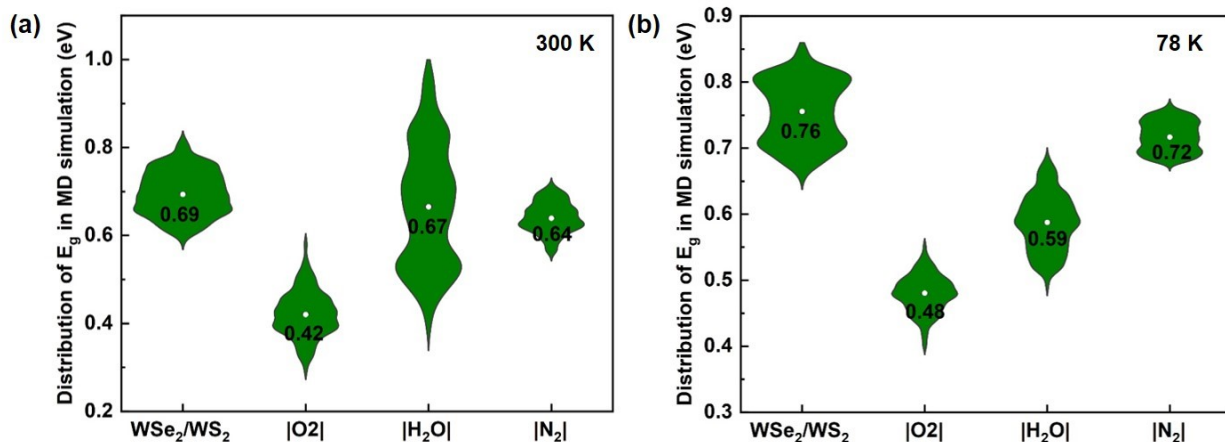


Figure S17. The band gap distribution during MD simulation of pristine, O_2 intercalated, H_2O intercalated and N_2 intercalated WSe_2/WS_2 vdW heterostructures at (a) 300 K and (b) 78 K, respectively. The average PBE band gap values are labeled in the center.

As shown in Figure S17, we plot the band gap distribution during MD simulation, and the average band gap of pristine, O_2 , H_2O and N_2 intercalated heterostructures are reduced compared with the static computation. The average band gaps of pristine, O_2 , H_2O and N_2 intercalated heterostructures are 0.69 eV, 0.42 eV, 0.67 eV and 0.64 eV, respectively. The average band gaps of pristine, O_2 intercalated, H_2O intercalated and N_2 intercalated heterostructures at 78 K are 0.76 eV, 0.48 eV, 0.59 eV and 0.72 eV as shown in Figure S17b.

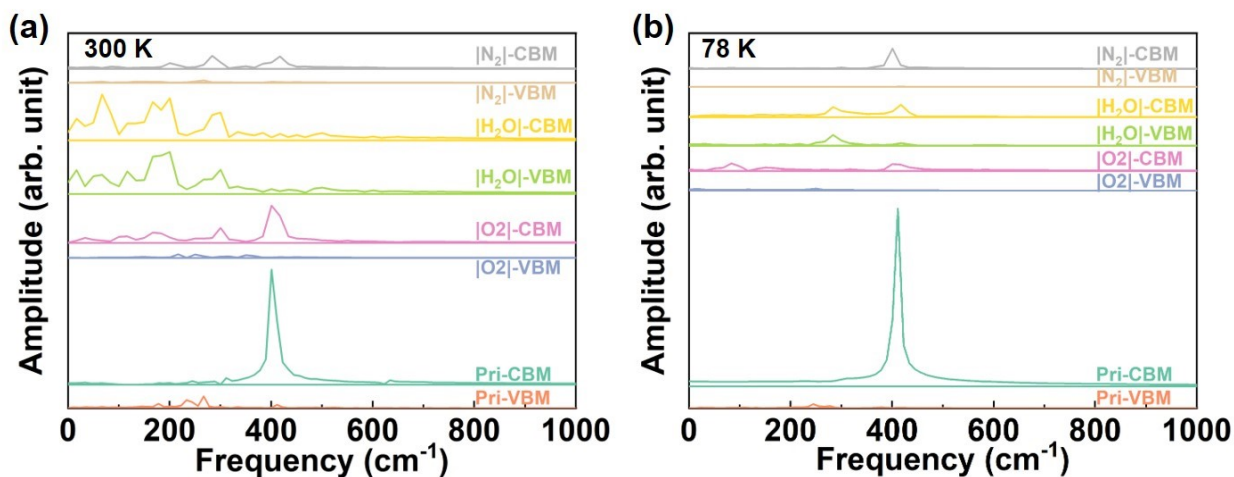


Figure S18. Fourier transforms of CBM and VBM of pristine, O₂ intercalated, H₂O intercalated and N₂ intercalated heterostructures at (a) 300 K and (b) 78 K, respectively.

As shown in Figure S18a, the relative phonon amplitude of CBM and VBM state of pristine, O₂ intercalated, H₂O intercalated and N₂ intercalated heterostructures at 300 K are plotted. It can be seen that after molecule intercalation, the phonon amplitudes of CBM state and VBM state are reduced indicating the smaller phonon occupation and weaker electron-phonon coupling element. The relative phonon amplitude of CBM and VBM state of pristine, O₂ intercalated, H₂O intercalated and N₂ intercalated heterostructures at 78 K is shown in Figure S18b. After molecule intercalation, the phonon amplitude of CBM state and VBM state is reduced significantly compared with pristine heterostructure, indicating the smaller phonon occupation and weaker electron-phonon coupling element.

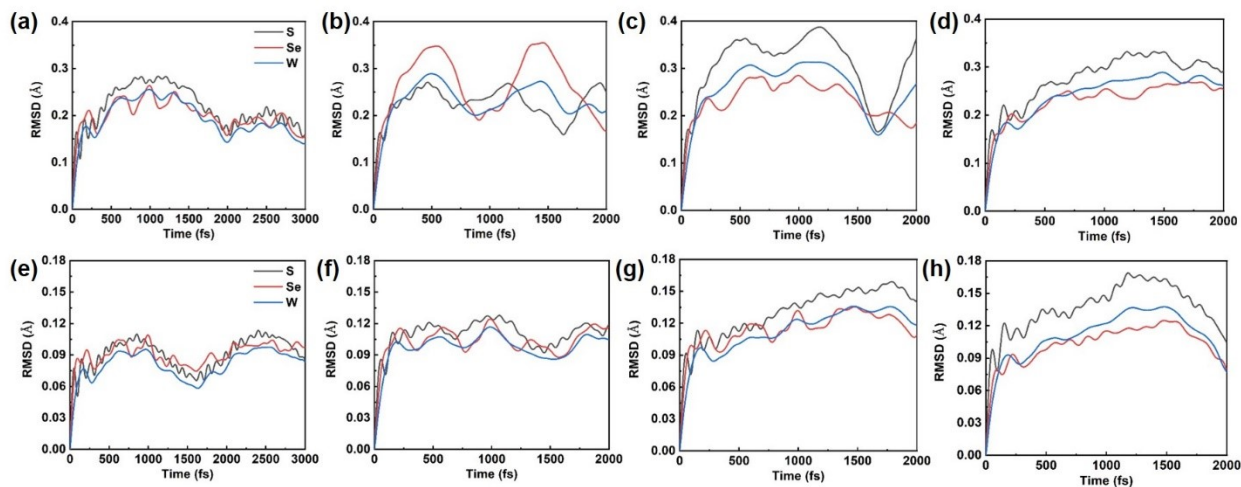


Figure S19. The RMSD of S, Se and W atoms during MD simulation of (a, e) pristine, (b, f) O_2 intercalated, (c, g) H_2O intercalated and (d, h) N_2 intercalated WSe_2/WS_2 vdW heterostructures at 300 K and 78 K, respectively.

The time dependent RMSD of pristine, O_2 intercalated, H_2O intercalated and N_2 intercalated heterostructures at 300 K is shown in Figure S19a-d, respectively. It can be seen that, O_2 intercalated, H_2O intercalated and N_2 intercalated heterostructures have the larger RMSD than pristine heterostructure indicating the larger nuclear velocity which expect to lead the larger NAC values. The RMSD of pristine, O_2 , H_2O and N_2 intercalated heterostructures at 78 K are shown in Figure S19e-h. Molecule intercalation increases RMSD, indicating larger nuclear velocity.

References

- 1 G. Kresse and J. Furthmüller, *Phys. Rev. B*, 1996, **54**, 11169.
- 2 G. Kresse and D. Joubert, *Phys. Rev. B*, 1999, **59**, 1758.
- 3 J. P. Perdew, K. Burke and M. Ernzerhof, *Phys. Rev. Lett.*, 1996, **77**, 3865.
- 4 H. Zeng, X. Liu, H. Zhang and X. Cheng, *Phys. Chem. Chem. Phys.*, 2021, **23**, 694-701.
- 5 H. J. Monkhorst and J. D. Pack, *Phys. Rev. B*, 1976, **13**, 5188-5192.
- 6 Q. Zheng, W. Chu, C. Zhao, L. Zhang, H. Guo, Y. Wang, X. Jiang and J. Zhao, *WIREs Comput. Mol. Sci.*, 2019, **9**, e1411.
- 7 J. C. Tully, *J. Chem. Phys.*, 1990, **93**, 1061-1071.
- 8 H. M. Jaeger, S. Fischer and O. V. Prezhdo, *J. Chem. Phys.*, 2012, **137**, 22A545.
- 9 G. Bussi, D. Donadio and M. Parrinello, *J. Chem. Phys.*, 2003, **119**, 2481.
- 10 A. Togo and I. Tanaka, *Scr. Mater.*, 2015, **108**, 1-5.